crystals

MDPI

Article

Influence of Alkyl Trimethyl Ammonium Bromides on Hydrothermal Formation of α-$CaSO_4 \cdot 0.5H_2O$ Whiskers with High Aspect Ratios

Ruosong Chen, Sichao Hou, Jing Wang * and Lan Xiang *

Department of Chemical Engineering, Tsinghua University, Beijing 100084, China; chenruosongxz@163.com (R.C.); 13718904065@126.com (S.H.)

* Correspondence: wangjingflotu@gmail.com (J.W.); xianglan@mail.tsinghua.edu.cn (L.X.); Tel.: +86-10-6278-8984 (J.W. & L.X.); Fax: +86-10-6277-2051 (J.W. & L.X.)

Academic Editor: Helmut Cölfen

Received: 1 December 2016; Accepted: 16 January 2017; Published: 18 January 2017

Abstract: In this paper, the influence of alkyl trimethyl ammonium bromides ($C_nH_{2n+1}(CH_3)_3NBr$, n = 10, 12, 14, 16, 18, abbreviated as ATAB) on the formation of alpha calcium sulfate hemihydrate (α-$CaSO_4 \cdot 0.5H_2O$) whiskers under a hydrothermal condition (135 °C, 3.0 h) was analyzed. Specifically, it focuses on cetyl trimethyl ammonium bromide ($C_{16}H_{33}(CH_3)_3NBr$, abbreviated as CTAB). The rising CTAB concentration from 0 to 9.2×10^{-4} mol·L^{-1} led to the increase of the average aspect ratio of α-$CaSO_4 \cdot 0.5H_2O$ whiskers from 80 to 430, since the selective adsorption of CTAB on the negatively-charged side facets of the whiskers inhibited the growth of the whiskers along the direction normal to the lateral facets. The further increase of CTAB concentration above the critical micelle concentration (abbreviated as CMC) showed little effect on the morphology of α-$CaSO_4 \cdot 0.5H_2O$ whiskers, considering that CTAB tended to form micelles instead of being adsorbed on the whisker surfaces. Similar phenomena were observed in other ATABs (n = 10, 12, 14, 18).

Keywords: α-$CaSO_4 \cdot 0.5H_2O$ whiskers; aspect ratio; CTAB; adsorption; critical micelle concentration

1. Introduction

Calcium sulfate whiskers with high aspect ratios are promising reinforcing materials for composites as rubbers, plastics, plaster and friction materials, etc. [1–4], showing excellent thermal stability and mechanical strength [5–7]. Calcium sulfate whiskers can be produced by preparing α-$CaSO_4 \cdot 0.5H_2O$ whiskers through hydrothermal, acidification, reverse micro-emulsion, and microwave-assisted approaches [8–13] followed by calcination of the α-$CaSO_4 \cdot 0.5H_2O$ whiskers above 600 °C [14,15]. Compared with the other methods, the hydrothermal route was widely used thanks to its moderate conditions and easily controlled parameters and whisker properties [16].

Ca^{2+} ions and $SO_4{}^{2-}$ tetrahedrons are stacked along the [001] direction and attached $-Ca-SO_4-Ca-SO_4-Ca-SO_4-$ chains in α-$CaSO_4 \cdot 0.5H_2O$ lattice. The chains form a framework parallel to the [001] direction with continuous channels, where the water molecules are combined and interact with $-Ca-SO_4-Ca-SO_4-Ca-SO_4-$ chains via hydrogen bonds. This crystal structure is favorable to the one-dimensional growth of α-$CaSO_4 \cdot 0.5H_2O$ whiskers along the c-axis [17–20]. The distribution of $SO_4{}^{2-}$ ions on the side facets as (200), (400), and (020) is denser than that of Ca^{2+} ions, while the distribution of Ca^{2+} ions on the top facet as (001) is denser than that of $SO_4{}^{2-}$ ions. Therefore, the side facets and top facet of the α-$CaSO_4 \cdot 0.5H_2O$ crystal are negatively and positively charged, respectively [18].

Many studies have been conducted in the effort to synthesize α-$CaSO_4 \cdot 0.5H_2O$ whiskers with high aspect ratios or varying morphologies, since the elasticity modulus of one-dimensional materials with homogeneous structures increases with increasing aspect ratios [21]. For example, Zhao et al. produced α-$CaSO_4{\cdot}0.5H_2O$ whiskers with an aspect ratio of 240 at 140 °C in the presence of $AlCl_3$, because the adsorption of Al^{3+} on the negatively charged side facets of the whiskers inhibited the growth of the whiskers along the direction normal to the lateral facets [22]. Hou et al. produced α-$CaSO_4{\cdot}0.5H_2O$ whiskers with an aspect ratio of up to 370 in the presence of 1.97×10^{-3} mol·L^{-1} $MgCl_2$ due to the adsorption and doping effects of Mg^{2+} on the side facets of the whiskers [23]. Based on the adsorption and inhibition mechanism, previous work focused on studying the influence of inorganic ions on the growth of α-$CaSO_4{\cdot}0.5H_2O$ whiskers, aimed at preparing the whiskers with high aspect ratios. Alkyl trimethyl ammonium bromides ($C_nH_{2n+1}(CH_3)_3NBr$, *n* = 10, 12, 14, 16, 18, abbreviated as ATAB) are commonly-used cation surfactants that may inhibit the growth of the whiskers along the direction normal to the lateral facets more effectively. They have long alkyl chains, which possibly provide a strong steric hindrance and reduce the surface energy of the side facets of the whiskers. Currently, the influence of ATABs on the hydrothermal formation of α-$CaSO_4{\cdot}0.5H_2O$ whiskers has yet to be reported.

In this work, a facile method was employed to synthesize α-$CaSO_4{\cdot}0.5H_2O$ whiskers with high aspect ratios by hydrothermal treatment of $CaSO_4{\cdot}2H_2O$ precursor at 135 °C in the presence of trace amount of CTAB (cetyl trimethyl ammonium bromide, $C_{16}H_{33}(CH_3)_3NBr$). For the first time, α-$CaSO_4{\cdot}0.5H_2O$ whiskers with an average aspect ratio of up to 430 were obtained. The influence of CTAB on the aspect ratios of α-$CaSO_4{\cdot}0.5H_2O$ whiskers was investigated, along with the corresponding mechanism. In addition, the effects of ATABs with varying alkyl chain lengths on the formation of α-$CaSO_4{\cdot}0.5H_2O$ whiskers was analyzed.

2. Results and Discussion

2.1. Influence of CTAB on the Formation of α-$CaSO_4{\cdot}0.5H_2O$ Whiskers

Figure 1 shows the XRD pattern and morphology of the $CaSO_4{\cdot}2H_2O$ raw material after calcination and hydration treatment. The XRD peaks were indexed to $CaSO_4{\cdot}2H_2O$ (JCPDS 33-0311). The activated $CaSO_4{\cdot}2H_2O$ was composed of irregular rectangle planes with a length of 2.0–8.0 μm and a width of 0.5–5.0 μm.

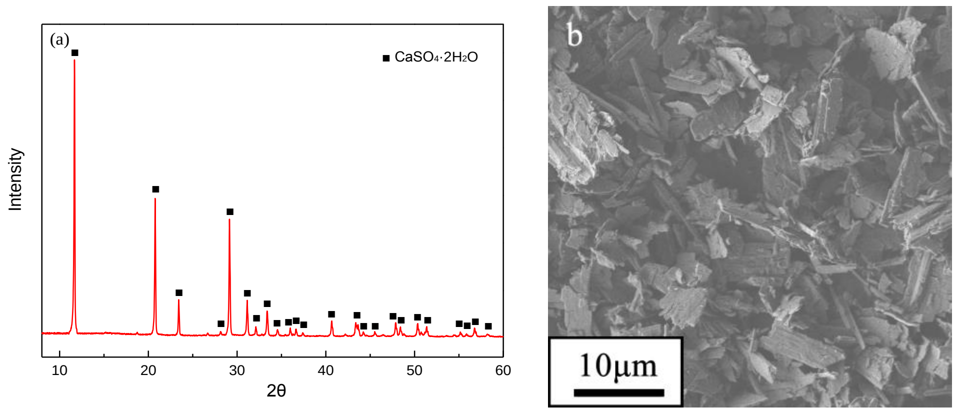

Figure 1. (**a**) XRD pattern and (**b**) SEM image of $CaSO_4{\cdot}2H_2O$ after calcination and hydration treatment.

Figures 2 and 3 show the morphology and aspect ratio distributions of the α-$CaSO_4{\cdot}0.5H_2O$ whiskers formed in the presence of 0–1.5×10^{-3} mol·L^{-1} CTAB. Whiskers with an average aspect ratio of 80 were prepared in the absence of CTAB (Figures 2a and 3a). The increase of the CTAB concentration from 1.0×10^{-4} to 9.2×10^{-4} mol·L^{-1} led to the gradual increase of the average aspect ratio of the whiskers from 240 to 430 ((Figures 2b,c and 3b,c). Little change in the aspect ratios was observed when further increasing the CTAB concentration (Figures 2d and 3d). TEM and high-resolution TEM

(HRTEM) images (Figure 2e,f) reveal that the inter-planar spacing parallel to the axial direction of the whiskers was 0.598 nm (corresponding to the spacing of (002) plane (0.599 nm) of α-$CaSO_4{\cdot}0.5H_2O$), indicating the intrinsic preferential growth of the whiskers along the c axis. The diffraction spots in the SAED pattern (Figure 2f) could be indexed to the $[1\bar{1}0]$ zone axis of α-$CaSO_4{\cdot}0.5H_2O$, reconfirming the preferential growth of the whiskers along the c axis.

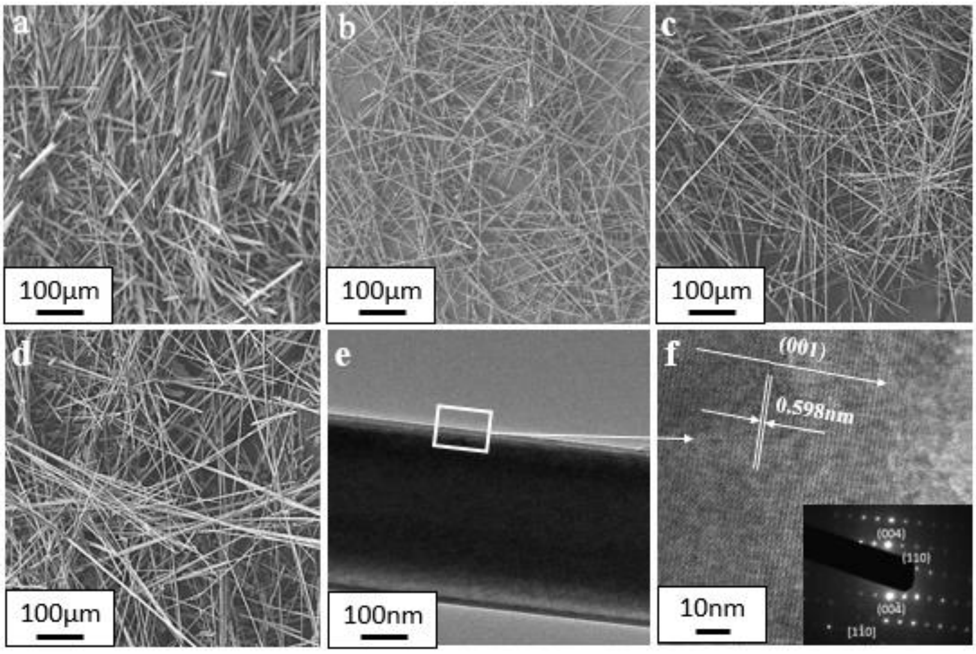

Figure 2. (**a**–**d**) SEM, (**e**) TEM, and (**f**) high-resolution TEM (HRTEM) images of α-$CaSO_4{\cdot}0.5H_2O$ whiskers CTAB (cetyl trimethyl ammonium bromide, $C_{16}H_{33}(CH_3)_3NBr$) (mol·L^{-1}): (**a**) 0; (**b**) 1.0×10^{-4}; (**c**,**e**,**f**) 9.2×10^{-4}; (**d**) 1.5×10^{-3}.

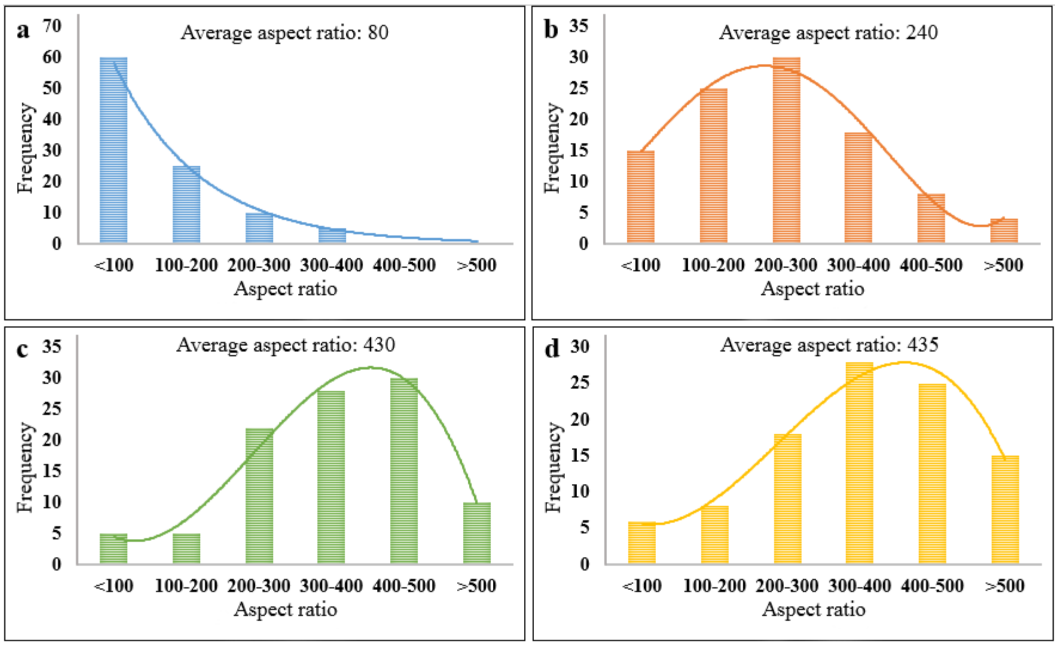

Figure 3. Influence of CTAB on the aspect ratios of α-$CaSO_4{\cdot}0.5H_2O$ whiskers CTAB (mol·L^{-1}): (**a**) 0; (**b**) 1.0×10^{-4}; (**c**) 9.2×10^{-4}; (**d**) 1.5×10^{-3}.

2.2. Adsorption of CTAB on α-$CaSO_4 \cdot 0.5H_2O$ Whiskers

The previous work showed that the side facets of α-$CaSO_4 \cdot 0.5H_2O$ whiskers are negatively charged, while the top facets of the whiskers are positively charged [18,24]. As a cationic surfactant, CTAB could possibly be adsorbed on the side facets of α-$CaSO_4 \cdot 0.5H_2O$ whiskers by electrostatic interactions. Figure 4 presents the variations of Fourier transform infrared (FT-IR) spectra and zeta potentials of the α-$CaSO_4 \cdot 0.5H_2O$ whiskers with CTAB concentration. As shown in Figure 4a, the peak at 660 cm^{-1} corresponded to the bending (ν_4) mode of SO_4^{2-}, while the peaks at 1620 cm^{-1} and 1685 cm^{-1} derived from the stretching (ν_2) mode of water in α-$CaSO_4 \cdot 0.5H_2O$. The peaks at 2850 cm^{-1} and 2920 cm^{-1} were ascribed to the stretching of C–H bonds in CTAB, the intensities of which increased with the CTAB concentration in the range of 0 to 9.2×10^{-4} mol·L^{-1} and remained unchanged when the CTAB concentration rose to 1.5×10^{-3} mol·L^{-1}. This indicated the adsorption of CTAB on the negatively-charged side facets of the whiskers. The zeta potential of the whiskers formed in the absence of CTAB declined from −8.05 to −20.92 mV as the pH increased from 2.52 to 10.44 (curve 1), revealing that the surfaces of the whiskers were negatively charged. The increase of zeta potentials with the CTAB concentration in the range of 0–9.2×10^{-4} mol·L^{-1} should be attributed to the enhanced adsorption of cationic CTAB on the negatively-charged side facets ((200), (400), and (020)) of the whiskers by electrostatic interactions, which provided a strong steric hindrance and inhibited the growth of the whiskers along the direction normal to the lateral facets.

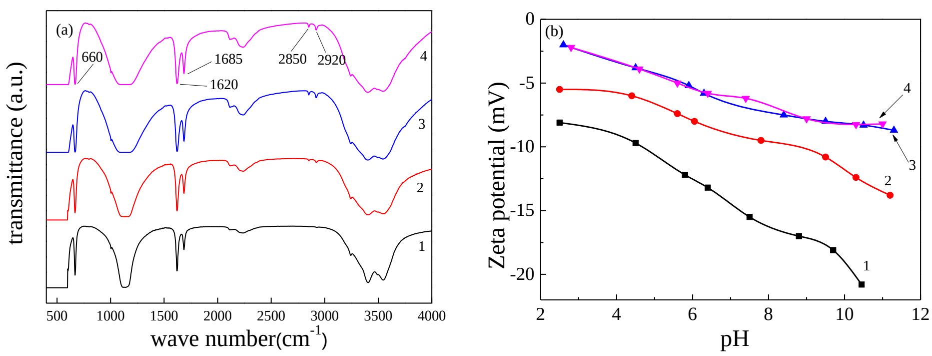

Figure 4. Variations of (**a**) Fourier transform infrared (FT-IR) spectra and (**b**) zeta potentials of α-$CaSO_4 \cdot 0.5H_2O$ whiskers with the CTAB concentration (mol·L^{-1}): 1—0, 2—1.0×10^{-4}, 3—9.2×10^{-4}, 4—1.5×10^{-3}.

The surface energy of the whiskers was influenced by the adsorption of CTAB. It was calculated by measuring the contact angles of water and CH_2I_2 on the whisker film. As shown in Table 1, the increase of CTAB led to the decline of the polar component of the surface energy and the decrease of the total surface energy (even if the dispersive component increased a little). Considering that CTAB was adsorbed on the side facets of the whiskers, it can be deduced that the decrease of the whisker surface energy was caused by the decrease of the surface energy of the side facets. The lower surface energy implied the increased stability of the side facets, which reduced the growth tendency of the whiskers along the direction normal to the lateral facets. In summary, the adsorption of CTAB on the side facets of the whiskers not only provided a strong steric hindrance preventing the addition of Ca^{2+} and SO_4^{2-}, but also reduced the surface energy of the side facets. Both aspects inhibited the growth of the whiskers along the direction normal to the lateral facets and led to the formation of α-$CaSO_4 \cdot 0.5H_2O$ whiskers with high aspect ratios.

As observed, the saturated adsorption seemed to occur when the CTAB concentration exceeded 9.2×10^{-4} mol·L^{-1}, which was shown by the unchanged zeta potential and the aspect ratios. The adsorption quantity of CTAB by α-$CaSO_4 \cdot 0.5H_2O$ whiskers was quantitatively analyzed by determining the dissociative CTAB in the reaction filtrate by an ultraviolet spectrophotometer. Figure 5 shows the variation of the adsorption quantity of CTAB on the whiskers with the CTAB concentration.

The adsorption quantity of CTAB increased almost linearly with the increase of the CTAB concentration in the range of 0–9.2 × 10^{-4} mol·L^{-1}, and the dissociative CTAB in the solution was negligible compared with the adsorbed CTAB. The adsorption reached saturation at 9.2 × 10^{-4} mol·L^{-1}, which is quite close to the critical micelle concentration (CMC) of CTAB. Based on the above results, the effects of CTAB were summarized and schematically illustrated in Figure 6. CTAB may be adsorbed mostly on the negatively charged side facets of the whiskers as free cationic ions when its concentration was less than the CMC, thus promoting the anisotropic growth of the whiskers along the c-axis; while the extra CTAB tended to form micelles in the solution instead of being adsorbed on the whisker surfaces when its concentration was greater than the CMC; this was why the whisker morphology and the adsorption quantity of CTAB remained unchanged when the CTAB concentration was greater than 9.2 × 10^{-4} mol·L^{-1}.

Table 1. Surface energy and polar and dispersive components of α-$CaSO_4$·0.5H_2O whiskers.

CTAB (mol·L^{-1})	θ (Water) (°)	θ (CH_2I_2) (°)	Polar Component (mN·m^{-1})	Dispersive Component (mN·m^{-1})	Surface Energy (mN·m^{-1})
0	14.700	18.013	39.279	33.085	72.364
1.0 × 10^{-4}	25.468	16.438	34.359	34.452	68.811
9.2 × 10^{-4}	32.586	15.533	30.165	35.594	65.759
1.5 × 10^{-3}	33.336	15.239	29.649	35.776	65.425

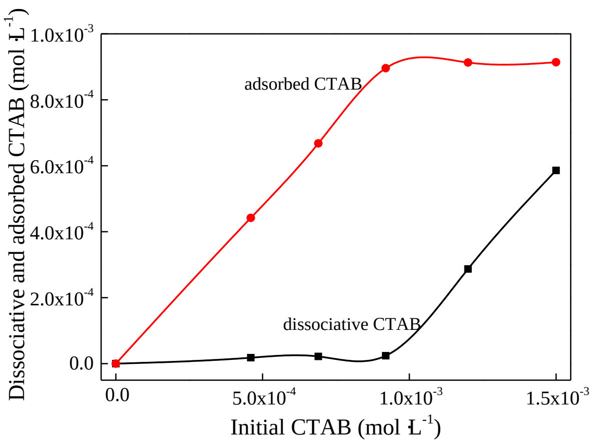

Figure 5. The dissociative and adsorbed CTAB after the hydrothermal reaction.

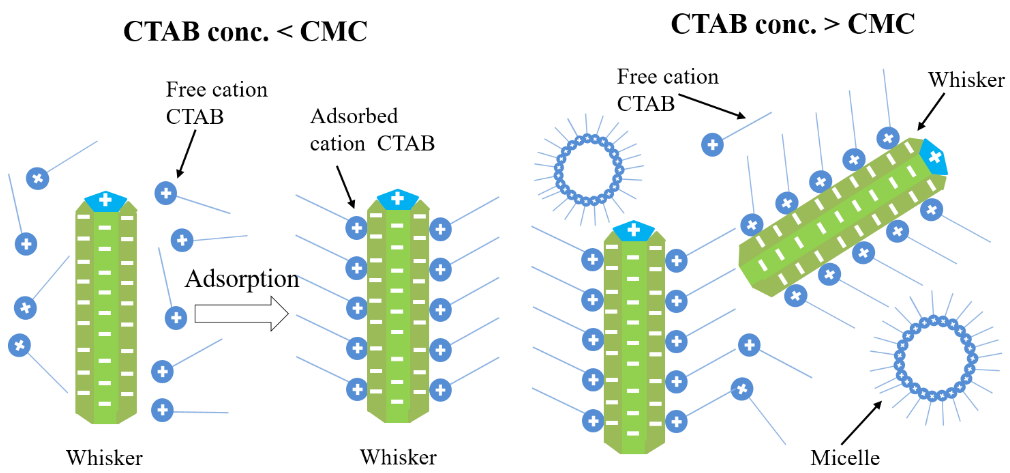

Figure 6. Adsorption sketch of CTAB on α-$CaSO_4$·0.5H_2O whisker surfaces. CMC: critical micelle concentration.

2.3. Influence of ATABs on α-$CaSO_4 \cdot 0.5H_2O$ Whiskers

The effect of CTAB on the formation of α-$CaSO_4 \cdot 0.5H_2O$ whiskers could also be extended to the other ATABs with varying alkyl chain lengths ($C_nH_{2n+1}(CH_3)_3NBr$, n = 10, 12, 14, 18). Figure 7 shows the variations of the aspect ratios of the whiskers with the ATAB concentration and alkyl chain length. The aspect ratios of the whiskers increased with increasing ATAB concentration, achieving its maximum at the CMCs of ATABs (indicated by the dashed line). The aspect ratios of the whiskers obtained at the CMCs increased approximately linearly with the alkyl chain length of ATABs. This may be attributed to the enhanced steric hindrance in ATABs with longer alkyl chains.

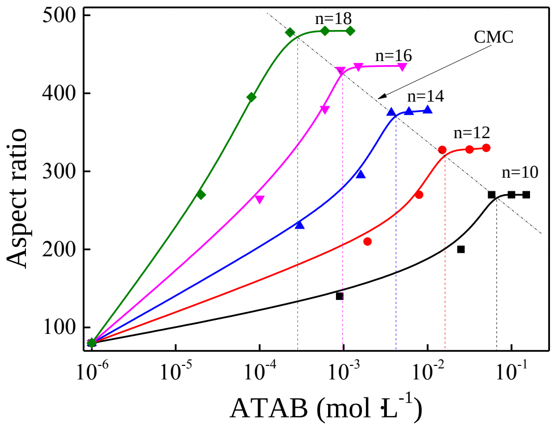

Figure 7. Influence of alkyl trimethyl ammonium bromides ($C_nH_{2n+1}(CH_3)_3NBr$, ATABs) on the aspect ratios of α-$CaSO_4 \cdot 0.5H_2O$ whiskers.

3. Materials and Methods

Commercial chemicals of analytical grade and deionized water with a resistivity >18 MΩ·cm^{-1} were used in the experiments. Calcium sulfate dihydrate ($CaSO_4 \cdot 2H_2O$, 99%) was purchased from Tianjin Fuchen Chemical Reagents Factory (Tianjin, China). Decyl trimethyl ammonium bromide ($C_{13}H_{30}BrN$, 99%), dodecyl trimethyl ammonium bromide ($C_{15}H_{34}BrN$, 99%), tetradecyl trimethyl ammonium bromide ($C_{17}H_{38}BrN$, 99%), cetyl trimethyl ammonium bromide ($C_{19}H_{42}BrN$, 99%), and octadecyl trimethyl ammonium bromide ($C_{21}H_{46}BrN$, 99%) were purchased from Sinopharm Chemical Reagent Co., Ltd. (Beijing, China). Ethanol (CH_3CH_2OH, 99.7%) was purchased from Beijing Tong Guang Fine Chemicals Company (Beijing, China). All of the chemicals were used without any further purification.

$CaSO_4 \cdot 2H_2O$ was calcined at 150 °C for 5.0 h followed by hydration in deionized water at 25 °C for 1.0 h. Then, 0.4 g of the calcination–hydration-treated $CaSO_4 \cdot 2H_2O$ was mixed at room temperature with 40.0 g of deionized water and a minor amount of ATABs with an alkyl chain length of 10 to 18 to get suspensions containing 1.0 wt % $CaSO_4 \cdot 2H_2O$ and 0–1.5 × 10^{-3} mol·L^{-1} ATAB. Then, the suspensions were transferred to the Teflon-lined stainless steel autoclaves with a volume of 80 mL and stirred with magnetic stirrers at a speed of 200 r/min for 15 min. Then, the autoclaves were put into a homogeneous reactor and kept under hydrothermal conditions (135 °C) for 3.0 h. The products were filtered, washed three times with ethanol, and dried at 105 °C for 4.0 h.

The morphology and microstructure of the samples were characterized with a field emission scanning electron microscope (FESEM, JSM 7401F, JEOL, Hitachi, Tokyo, Japan) and a high-resolution transmission electron microscope (HRTEM, JEM-2010, JEOL, Hitachi, Tokyo, Japan) equipped with selected area electron diffraction (SAED). The average diameters and lengths of the whiskers were estimated by directly measuring about 200 whiskers from the typical FESEM images with the magnifications of 250–5000. The functional groups of the samples were examined using a Fourier transform infrared spectrometer (FT-IR, Nexus, Nicolet, Madison, MI, USA). The surface electric potentials of the samples were measured with a zeta potential analyzer (ZETAPALS, Brookhaven Instruments Corporation, Brookhaven, MS, USA) in the pH range of 2.0–13.0. The amount of the dissociative CTAB in the filtrate was determined with an ultraviolet spectrophotometer (U-3010, Hitachi, Tokyo, Japan).

The contact angles (θ) of deionized water and diiodomethane (CH_2I_2) on the surfaces of the whiskers were measured by a dynamic contact angle tensiometer (OCA20, Dataphysics, Filderstadt, Germany). The surface energy (γ_s^T) of the whiskers and its dispersive component (γ_s^d) and polar component (γ_s^p) were figured out by the following equation [24]: $\gamma_l^T(1+cos\theta) = 2\left(\gamma_l^d\gamma_s^d\right)^{0.5} + 2\left(\gamma_l^p\gamma_s^p\right)^{0.5}$, $\gamma_l^T = \gamma_l^d + \gamma_l^p$, $\gamma_s^T = \gamma_s^d + \gamma_s^p$, where γ_l^T, γ_l^d, γ_l^p are the surface energy of the immersion liquid, its dispersive component, and its polar component, respectively. For deionized water, γ_l^T = 72.8 mN·m^{-1}, γ_l^d = 21.8 mN·m^{-1}, and γ_l^p = 51.0 mN·m^{-1}. For diiodomethane, γ_l^T = 50.8 mN·m^{-1}, γ_l^d = 48.5 mN·m^{-1}, and γ_l^p = 2.3 mN·m^{-1}. Each measurement was repeated five times, and the average results were adopted.

4. Conclusions

α-$CaSO_4 \cdot 0.5H_2O$ whiskers with high aspect ratios were synthesized in the presence of CTAB. The increase of the CTAB concentration from 0 to 9.2 × 10^{-4} mol·L^{-1} (CMC) led to the increase of the average aspect ratio of the whiskers from 80 to 430. The adsorption of the positively charged cationic CTAB on the negatively charged side facets of the whiskers provided a strong steric hindrance and reduced the surface energy of the side facets, which favored the one-dimensional growth of the whiskers along the c-axis, promoting the formation of whiskers with high aspect ratios. When the CTAB concentration was greater than the CMC (9.2 × 10^{-4} mol·L^{-1}), the whisker morphology and the adsorption quantity of CTAB remained unchanged with the increase of the CTAB concentration, since the extra CTAB tended to form micelles instead of being adsorbed on the whisker surfaces. Similar phenomena were also observed in other ATABs with varying alkyl chain lengths ($C_nH_{2n+1}(CH_3)_3NBr$, n = 10, 12, 14, 18).

Acknowledgments: This work was financially supported by the National Science Foundation of China (Nos. 51234003 and 51374138) and National Key Technology Research and Development Program of China (2013BAC14B02).

Author Contributions: Ruosong Chen and Sichao Hou conceived and designed the experiments; Ruosong Chen performed the experiments; Sichao Hou and Ruosong Chen analyzed the data; Ruosong Chen, Jing Wang and Lan Xiang wrote the paper.

Conflicts of Interest: The authors declare no conflict of interest.

References

1. Ru, X.; Ma, B.; Huang, J.; Huang, Y. Phosphogypsum Transition to α-Calcium Sulfate Hemihydrate in the Presence of Omongwaite in NaCl Solutions Under Atmospheric Pressure. *J. Am. Ceram. Soc.* **2012**, *95*, 3478–3482. [CrossRef]
2. Tritschler, U.; Alexander, E.S.; Kempter, A.; Kellermeier, M.; Cölfen, H. Controlling the Selective Formation of Calcium Sulfate Polymorphs at Room Temperature. *Angew. Chem. Int. Ed.* **2015**, *54*, 4083–4086. [CrossRef] [PubMed]
3. Mao, X.; Song, X.; Lu, G.; Sun, Y.; Xu, Y.; Yu, J. Control of Crystal Morphology and Size of Calcium Sulfate Whiskers in Aqueous HCl Solutions by Additives: Experimental and Molecular Dynamics Simulation Studies. *Ind. Eng. Chem. Res.* **2015**, *54*, 4781–4787. [CrossRef]
4. Wang, H.; Mu, B.; Ren, J.; Jian, L.; Zhang, J.; Yang, S. Mechanical and Tribological Behaviors of PA66/PVDF Blends Filled with Calcium Sulfate Whiskers. *Polym. Compos.* **2009**, *30*, 1326–1332. [CrossRef]
5. Xu, A.; Li, H.; Luo, K.; Xiang, L. Formation of Calcium Sulfate Whiskers from $CaCO_3$-Bearing Desulfurization Gypsum. *Res. Chem. Intermed.* **2011**, *37*, 449–455. [CrossRef]

6. Capadona, J.R.; Shanmuganathan, K.; Trittschuh, S.; Seidel, S.; Rowan, S.J.; Weder, C. Polymer Nanocomposites with Nanowhiskers Isolated from Microcrystalline Cellulose. *Biomacromolecules* **2009**, *10*, 712–716. [CrossRef] [PubMed]
7. Liu, J.; Reni, L.; Wei, Q.; Wu, J.; Liu, S.; Wang, Y.; Li, G. Fabrication and Characterization of Polycaprolactone/Calcium Sulfate Whisker Composites. *Express Polym. Lett.* **2011**, *5*, 742–752. [CrossRef]
8. Luo, K.; Li, C.; Xiang, L.; Li, H.; Ning, P. Influence of Temperature and Solution Composition on the Formation of Calcium Sulfates. *Particuology* **2010**, *8*, 240–244. [CrossRef]
9. Wang, Y.; Kim, Y.; Christenson, H.K.; Meldrum, F.C. A new precipitation pathway for calcium sulfate dihydrate (gypsum) via amorphous and hemihydrate intermediates. *Chem. Commun.* **2012**, *48*, 504–506. [CrossRef] [PubMed]
10. Kong, B.; Guan, B.; Yates, M.Z.; Wu, Z. Control of α-Calcium Sulfate Hemihydrate Morphology Using Reverse Microemulsions. *Langmuir* **2012**, *28*, 14137–14142. [CrossRef] [PubMed]
11. Chen, Y.; Wu, Q.; Ding, Y. Stepwise Assembly of Nanoparticles, -tubes, -rods, and -wires in Reverse Micelle Systems. *Eur. J. Inorg. Chem.* **2007**, 4906–4910. [CrossRef]
12. Guan, B.; Ma, X.; Wu, Z.; Yang, L.; Shen, Z. Crystallization Routes and Metastability of α-Calcium Sulfate Hemihydrate in Potassium Chloride Solutions under Atmospheric Pressure. *J. Chem. Eng. Data* **2009**, *54*, 719–725. [CrossRef]
13. Li, L.; Zhu, Y.; Ma, M. Microwave-assisted Preparation of Calcium Sulfate Nanowires. *Mater. Lett.* **2008**, *62*, 4552–4554. [CrossRef]
14. Singh, N.B.; Middendorf, B. Calcium Sulphate Hemihydrate Hydration Leading to Gypsum Crystallization. *Prog. Cryst. Growth Charact. Mater.* **2007**, *53*, 57–77. [CrossRef]
15. McAdie, H.G. The Effect of Water Vapor upon the Dehydration of $CaSO_4 \cdot 2H_2O$. *Can. J. Chem.* **1964**, *42*, 792–801. [CrossRef]
16. Chen, H.; Wang, J.; Hou, S.; Xiang, L. Influence of NH_4Cl on Hydrothermal Formation of α-$CaSO_4 \cdot 0.5H_2O$ Whiskers. *J. Nanomater.* **2015**. [CrossRef]
17. Ballirano, P.; Maras, A.; Meloni, S.; Caminiti, R. The Monoclinic I2 Structure of Bassanite, Calcium Sulphate Hemihydrate ($CaSO_4 \cdot 0.5H_2O$). *Eur. J. Mineral.* **2001**, *13*, 985–993. [CrossRef]
18. Xin, Y.; Xiang, L.; Yu, Y. Influence of structure on the morphology of $CaSO_4 \cdot nH_2O$ (n = 0, 0.5, 2): A molecular simulation study. *Mater. Res. Innov.* **2015**, *19*, 103–107. [CrossRef]
19. Bezou, C.; Nonat, A.; Mutin, J.C. Investigation of the Crystal Structure of γ-$CaSO_4$, $CaSO_4 \cdot 0.5H_2O$, and $CaSO_4 \cdot 0.6H_2O$ by Powder Diffraction Methods. *J. Solid State Chem.* **1995**, *117*, 165–176. [CrossRef]
20. Freyer, D.; Voigt, W. Crystallization and Phase Stability of $CaSO_4$ and $CaSO_4$-Based Salts. *Monatshefte Chem.* **2003**, *134*, 693–719. [CrossRef]
21. Muscolino, G.; Sofi, A.; Zingales, M. One-dimensional heterogeneous solids with uncertain elastic modulus in presence of long-range interactions: Interval versus stochastic analysis. *Comput. Struct.* **2013**, *122*, 217–229. [CrossRef]
22. Zhao, W.; Gao, C.; Zhang, G.; Xu, J.; Wang, C.; Wu, Y. Controlling the morphology of calcium sulfate hemihydrate using aluminum chloride as a habit modifier. *New J. Chem.* **2016**, *40*, 3104–3108. [CrossRef]
23. Hou, S.; Wang, J.; Wang, X.; Chen, H.; Xiang, L. Effect of Mg^{2+} on Hydrothermal Formation of α-$CaSO_4 \cdot 0.5H_2O$ Whiskers with High Aspect Ratios. *Langmuir* **2014**, *30*, 9804–9810. [CrossRef] [PubMed]
24. Wu, Z.; Meng, L.; Liu, L.; Jiang, Z.; Xing, L.; Jiang, D.; Huang, Y. Interfacial microstructure and properties of carbon fiber-reinforced unsaturated polyester composites modified with carbon nanotubes. *J. Adhes. Sci. Technol.* **2014**, *28*, 444–453. [CrossRef]